HD–THEP–94–13

CRITICAL BUBBLES AND FLUCTUATIONS AT THE ELECTROWEAK PHASE TRANSITION

Jochen Kripfganz[†1]

Andreas Laser[†]

Michael G. Schmidt[†*2]

[†]Institut für Theoretische Physik
Universität Heidelberg
Philosophenweg 16
D-69120 Heidelberg, FRG

[*]Theoretical Physics Division
CERN
CH-1211 Geneva 23, Switzerland

Abstract

We discuss the critical bubbles of the electroweak phase transition using an effective high-temperature 3-dimensional action for the Higgs field φ. The separate integration of gauge and Goldstone boson degrees of freedom is conveniently described in the 't Hooft-Feynman covariant background gauge. The effective dimensionless gauge coupling $g_3(T)^2$ in the broken phase is well behaved throughout the phase transition. However, the behavior of the one-loop $Z(\varphi)$ factors of the Higgs and gauge kinetic terms signalizes the breakdown of the derivative expansion and of the perturbative expansion for a range of small φ values increasing with the Higgs mass m_H. Taking a functional $S_z[\varphi]$ with constant $Z(\varphi) = z$ instead of the full non-local effective action in some neighborhood of the saddlepoint we are calculating the critical bubbles for several temperatures. The fluctuation determinant is calculated to high accuracy using a variant of the heat kernel method. It gives a strong suppression of the transition rate compared to previous estimates.

[1]supported by Deutsche Forschungsgemeinschaft
[2]on sabbatical leave

e-mail addresses:
J. Kripfganz dj8@vm.urz.uni-heidelberg.de
A. Laser t82@ix.urz.uni-heidelberg.de
M.G. Schmidt k22@vm.urz.uni-heidelberg.de

1 Introduction

There are strong indications [1] – [6] that the electroweak standard theory predicts a first-order phase transition at high temperatures corresponding to the electroweak scale. The critical bubbles of the transition are solutions of the static electroweak semiclassical equations of motion. The transition probability can be calculated using Langer's theory [7]. The exact production rate is important for the timing of the transition and the determination of the corresponding temperature. The baryon asymmetry of the universe may be generated through bubble expansion because the three Sakharov criteria – C/CP violation, baryon number violation and nonequilibrium – are fulfilled.

In a proper treatment of the electroweak phase transition the coarse-grained action constructed consistently for the particular problem and the size scale involved should be used. If there are different mass scales one can integrate out first the more massive fields and keep the light fields in an effective action relevant for the phase transition. At high temperature non-static Matsubara modes may be considered as heavy fields. Integrating out these modes leads to a 3-dimensional effective theory with symmetry restoration at high temperature. The related phase transition is predicted to be second-order instead of first-order, however. It becomes first-order due to contributions from static modes. So some of the light modes have to be integrated out as well in calculating the effective action. It is well known that integrating out the non-static modes using the high temperature expansions and then integrating out the static gauge boson fields one has already an effective potential leading to a first-order phase transition. In this spirit it is very natural to integrate out the static Goldstone modes as well. This is most conveniently done in the 't Hooft-Feynman covariant background gauge. With the pure real scalar background of the bubble configurations one ends up with a 3-dimensional effective Higgs action whose fluctuations still have to be considered.

If a small coupling parameter - maybe after some redefinitions - can be identified, the one-loop perturbative expansion for the effective action will be a good approximation. A carefully introduced gauge coupling $g_3(T)^2$ in the broken phase is well behaved throughout the phase transition, and indeed it is not very large for $m_H \leq m_W$.

The $Z_H(\varphi)$ factor of the Higgs kinetic term will be calculated explicitly in the 't Hooft-Feynman covariant background gauge in one-loop order. It differs considerably from that in the Landau gauge. Due to the fact that $Z_H(\varphi)$ is negative in some φ range, it is not sensible to include it in this form in the effective action. We will argue that the derivative expansion breaks down in this range.

We also inspect the one-loop $Z_{\rm gauge}(\varphi)$ prefactor of the kinetic gauge term. It plays no direct role in the bubble action. However, $g_3(T)^2/Z_{\rm gauge}(\varphi)$ is the effective gauge coupling at the constant scale φ. It blows up for $Z_{\rm gauge} \to 0$ and this happens already at rather large values of φ (> 0.4) for $m_H > \frac{1}{2}m_W$. Thus except for very small m_H the φ-range relevant for the bubble configuration may be largely nonperturbative in the effective gauge coupling. Integration of the (enlarged) gauge degrees of freedom to some (one) loop order can in this range at best be suggestive for the form of the effective Higgs action.

We will then consider a Higgs effective action with the known one-loop effective potential and a kinetic term with arbitrary constant Z factor. This allows us to come to our main subject, the discussion of radiative corrections in the heat kernel method. Since there is no background gauge field for the bubble configuration, the heat kernel expansion already exists to very high order (and can easily be extended using new methods [8, 9]). Thus we can arrive at a very precise treatment of the fluctuations.

It turns out that the static prefactor which is essentially the fluctuation determinant gives a strong suppression of the nucleation rate. Its logarithm may be interpreted as the one-loop correction to the effective action of the critical bubble. The comparison between the two values decides on the applicability of the nucleation theory.

Section 2 contains a discussion of the 3-dimensional effective high temperature Higgs action obtained from one-loop integration of all the other fields in the 't Hooft-Feynman background gauge and a critical inspection of derivative expansion and of perturbation theory. In section 3 we first shortly review the nucleation rate based on Langer's theory. We discuss the critical bubbles obtained with the modification mentioned above. In the following we consider the heat kernel method for calculating the fluctuation determinant and develop a particular method to treat zero/instable modes. We present our high accuracy results for the fluctuation prefactor in the transition rate. Section 4 gives our conclusion. Appendix A contains the calculation of Z factors, Appendix B some generalization of the thin-wall bubble solution. Appendix C gives the first six operators in the heat kernel expansion.

2 The Effective Action

The critical bubble solutions describing the first-order phase transition of the electroweak theory are pure Higgs field configurations. They are not solutions of the original fundamental field equations of the electroweak theory, but correspond to an effective action where (part of) the other field degrees of freedom have already been integrated out. It is the aim of the 'exact renormalization group approach' to derive such an action well adapted to the size of the bubbles. In the case of a gauge theory this demanding program is just being developed [10, 11]. Still a simpler way to discuss critical bubbles is to generate new terms of the Higgs effective action by using low-order perturbation theory, starting from the fundamental Lagrangian. However in a rigorous treatment this requires the identification of appropriate expansion parameters (which may not be possible).

2.1 The high-temperature effective action

In the case of the electroweak phase transition it is appropriate to perform a high temperature expansion. The expansion parameter is $m(T)/T$. The guiding principle is to integrate out the heavy field degrees of freedom to get an effective theory of the light fields.

In a first step it is possible to integrate out the non-static Matsubara-frequencies which gain masses proportional to the temperature T ($2n\pi T$ with $n \neq 0$ for bosons and $(2n+1)\pi T$ for fermions). The remaining effective theory is purely bosonic and 3-dimensional. As argued in ref. [12] the high-temperature dimensional reduction has shortcomings in higher orders of perturbation theory.

In a second step the longitudinal component A_0 of the gauge field is integrated out. It develops a Debye-mass proportional to gT.

In a third step we rescale the coordinates and fields

$$\vec{x} \to \frac{\vec{x}}{gv}, \qquad \Phi \to v\Phi, \qquad A \to vA \tag{2.1}$$

where the scale v is left open for the moment. The remaining high-temperature effective

action can be written, in the limit of vanishing electroweak mixing angle, as

$$S_{\rm ht} = \frac{1}{g_3(T)^2} \int d^3x \left[\frac{1}{4} F_{ij}^a F_{ij}^a + (D_i \Phi)^\dagger (D_i \Phi) + V_{\rm ht}(\Phi^\dagger \Phi) \right] \tag{2.2}$$

with other contributions vanishing powerlike at high temperature, e.g. a $(\Phi^\dagger\Phi)^3/T^2$ term. They have been discussed to be unimportant [4].

The effective 3-dimensional gauge coupling is defined as

$$g_3(T)^2 = \frac{gT}{v} \quad . \tag{2.3}$$

The gauge coupling g has been scaled out of the covariant derivative and the field strength tensor. The high-temperature effective potential is

$$V_{\rm ht}(\Phi^\dagger\Phi) = \frac{\lambda_T}{g^2} \left((\Phi^\dagger\Phi)^2 - \left(\frac{v_0(T)}{v} \right)^2 \Phi^\dagger\Phi \right) \quad . \tag{2.4}$$

$\frac{v_0(T)^2}{v^2}$ is the asymmetric minimum

$$v_0(T)^2 = \frac{2}{\lambda_T} \left(T_0^2 - T^2 \right) D \quad . \tag{2.5}$$

It is negative for $T > T_0$. At these temperatures the global minimum of $V_{\rm ht}(\Phi^\dagger\Phi)$ is the symmetric one at $\Phi^\dagger\Phi = 0$. At T_0 it moves continuously to finite values. Therefore this potential predicts a second-order phase transition.

The constants are determined by the parameters of the standard model. They can be calculated from the zero temperature masses $\tilde{m}$ and the zero temperature vacuum expectation value of the scalar field $\tilde{v} = 246$ GeV

$$\begin{aligned} \tilde{m}_W^2 &= \frac{1}{4} g^2 \tilde{v}^2, \qquad \tilde{m}_H^2 = 2\lambda \tilde{v}^2 \\ T_0^2 &= \frac{\tilde{m}_H^2 - 8\tilde{v}^2 B}{4D} \\ D &= \frac{1}{8\tilde{v}^2} (3\tilde{m}_W^2 + 2\tilde{m}_t^2) \\ B &= \frac{3}{64\pi^2 \tilde{v}^4} (3\tilde{m}_W^4 - 4\tilde{m}_t^4) \quad . \end{aligned} \tag{2.6}$$

The temperature dependent quartic coupling is

$$\begin{aligned} \lambda_T &= \lambda - \frac{3}{16\pi^2\tilde{v}^4} \left(3\tilde{m}_W^4 \log \frac{\tilde{m}_W^2}{a_B T^2} - 4\tilde{m}_t^4 \log \frac{\tilde{m}_t^2}{a_F T^2} \right) \\ & \ln(a_B) = 3.91, \qquad \ln(a_F) = 1.14 \quad . \end{aligned} \tag{2.7}$$

The theory described by eq. (2.2) is nothing but the 3-dimensional $SU(2)$ Higgs model; it has 13 field degrees of freedom; 9 from the gauge field and 4 from the scalar field.

2.2 Background field and fluctuations

The high-temperature potential in eq. (2.2) corresponds to a second-order phase transition. From lattice calculation [5, 6], however, and from the full one-loop effective potential [1]

– [4] one expects the electroweak phase transition to be first-order. This will be manifest by integrating out further degrees of freedom.

In most cases, a first-order phase transition is initiated by the formation of critical bubbles. The electroweak critical bubbles are pure real Higgs field configurations. We therefore divide the 13 remaining fields into the real background field φ and into fluctuations in the following way

$$\begin{aligned} A_i^a &\rightarrow A_i^a + g_3\, a_i^a \qquad A_i^a = 0 \\ \Phi &\rightarrow \Phi + g_3\phi \\ \Phi &= \sqrt{\frac{1}{2}}\begin{pmatrix} 0 \\ \varphi \end{pmatrix} \qquad \phi = \sqrt{\frac{1}{2}}\begin{pmatrix} \chi^1 + i\chi^2 \\ \eta + i\chi^3 \end{pmatrix} \quad . \end{aligned} \tag{2.8}$$

The fluctuations have to be gauge-fixed in some way. A class of covariant background gauges is given by

$$F^a = D_i(A)\, a_i^a + i\xi \left(\Phi^\dagger \frac{\sigma^a}{2}\phi - \phi^\dagger \frac{\sigma^a}{2}\Phi \right) = 0 \quad . \tag{2.9}$$

We use the 't Hooft-Feynman gauge where the gauge parameter is $\xi = 1$. This is contrary to most publications on the electroweak phase transitions which work in the Landau gauge.

Using eq. (2.8) and eq. (2.9) the high temperature action (eq. (2.2)) changes into

$$S_{\rm ht} + \frac{1}{2\xi}\int d^3x F^a F^a \;\rightarrow\; S_{\rm ht}^{\rm bg} + \delta S_{\rm lin} + \delta S_{\rm quad} + \ldots \tag{2.10}$$

with the background field part

$$S_{\rm ht}^{\rm bg} = \frac{1}{g_3(T)^2}\int d^3x \left[\frac{1}{2}\partial_i\varphi\partial_i\varphi + V_{\rm ht}(\varphi^2) \right] \quad . \tag{2.11}$$

The part which is linear in the fluctuations is proportional to η, the fluctuation which corresponds to the Higgs field φ (cf. eq. (2.8))

$$\delta S_{\rm lin} \propto \frac{1}{g_3(T)}\eta \quad . \tag{2.12}$$

There are no linear terms in the other fluctuations. This is due to the fact that the background field takes the minimum of this part of the fundamental action. Note that we already made use of the absence of linear terms in integrating out the non-static Matsubara-frequencies. Neglecting tadpoles here was only possible due to the fact that the remaining degrees of freedom are purely 3-dimensional.

The part quadratic in the fluctuations is most simply written in matrix notation

$$\begin{aligned} \delta S_{\rm quad} &= \frac{1}{2}\int d^3x \;\; Q^T \cdot \left[-\partial^2 \mathbf{1} + \begin{pmatrix} U & 0 & 0 & 0 \\ 0 & U & 0 & 0 \\ 0 & 0 & U & 0 \\ 0 & 0 & 0 & m_H^2 \end{pmatrix} \right] \cdot Q \\ Q^T &= \Big(a_1^1, a_2^1, a_3^1, \chi^1, \quad a_1^2, a_2^2, a_3^2, \chi^2, \quad a_1^3, a_2^3, a_3^3, \chi^3, \quad \eta \Big) \quad . \end{aligned} \tag{2.13}$$

U is a 4×4-matrix

$$U = U_0 + \delta U \tag{2.14}$$

$$U_0 = \begin{pmatrix} m_W^2 & 0 & 0 & 0 \\ 0 & m_W^2 & 0 & 0 \\ 0 & 0 & m_W^2 & 0 \\ 0 & 0 & 0 & m_\chi^2 \end{pmatrix} \qquad \delta U = \begin{pmatrix} 0 & 0 & 0 & \partial_1\varphi \\ 0 & 0 & 0 & \partial_2\varphi \\ 0 & 0 & 0 & \partial_3\varphi \\ \partial_1\varphi & \partial_2\varphi & \partial_3\varphi & 0 \end{pmatrix} \quad . \tag{2.15}$$

The diagonal elements are the finite temperature squared masses

$$m_H^2 = \frac{\lambda_T}{g^2}\left(3\varphi^2 - \left(\frac{v_0}{v}\right)^2\right) \tag{2.16}$$

$$m_\chi^2 = \frac{1}{4}\varphi^2 + \frac{\lambda_T}{g^2}\left(\varphi^2 - \left(\frac{v_0}{v}\right)^2\right) \tag{2.17}$$

$$m_W^2 = \frac{1}{4}\varphi^2 \tag{2.18}$$

$$m_{\rm gh}^2 = \frac{1}{4}\varphi^2 \quad . \tag{2.19}$$

They are positive in the range of phase transition, because $\left(\frac{v_0}{v}\right)^2$ is negative. In the broken phase they are of the same order of magnitude while gauge boson and ghost masses vanish in the symmetric phase. Hence there is no mass hierarchy which holds over the whole interesting φ-range.

Note that the η-fluctuation does not mix with the other fluctuations (eq. (2.13)). In addition there are no linear terms proportional to a_i^a or χ^a. In one-loop order it is therefore possible to perform the remaining integrations in two steps. In a first step we integrate out gauge fields, ghosts, and Goldstone bosons to get an effective action for the φ field. We might not find a local effective action through this procedure, however, because it is not supported by an appropriate mass hierarchy. Nevertheless we shall discuss a local expansion, because the relevant scale is set by the bubble solutions which will be calculated in section 3.2. Anticipating the results (figure 5) one sees that the corresponding mass which is given by the inverse wall thickness is quite small ($\approx \frac{1}{30} g v(T)$).

In a second step, the fluctuations of the φ field contributing to the static prefactor of the nucleation rate will be calculated.

2.3 The effective action of the Higgs field φ

The effective action of the Higgs field φ is in one-loop order calculated from

$$S_{\rm eff}[\varphi] = S_{\rm ht}^{\rm bg}[\varphi] + \delta S[\varphi] \tag{2.20}$$

with

$$\delta S = \frac{1}{2}\log\det(-\partial^2 + M_{12}) - \log\det(-\partial^2 + M_{\rm gh}) \quad . \tag{2.21}$$

The 12×12 a-χ-matrix M_{12} is a part of $\delta S_{\rm quad}$ (eq. (2.13)), while the 3×3 ghost-matrix $M_{\rm gh}$ is easily calculated from the gauge-fixing condition (eq. (2.9)).

$$M_{\rm gh} = \begin{pmatrix} m_{\rm gh}^2 & 0 & 0 \\ 0 & m_{\rm gh}^2 & 0 \\ 0 & 0 & m_{\rm gh}^2 \end{pmatrix} \tag{2.22}$$

The derivative expansion can be carried out by calculating Feynman diagrams, by summing up the relevant contributions of the heat-kernel expansion, or by using a method proposed in ref. [13]. The latter is explained in more detail in appendix A. The three methods of course yield identical results.

One gets the effective action

$$S_{\rm eff}[\varphi] = \frac{1}{g_3(T)^2}\int d^3x \left[V_{\rm eff}(\varphi) + \frac{1}{2}Z_H(\varphi)\partial_i\varphi\partial_i\varphi + \mathcal{O}(\partial\varphi^4)\right] \tag{2.23}$$

with the effective potential

$$V_{\rm eff}(\varphi) = V_{\rm ht} - \frac{g_3(T)^2}{12\pi}\left(9m_W^3 - 6m_{\rm gh}^3 + 3m_\chi^3\right) \quad (2.24)$$

$$= \frac{\lambda_T}{g^2}\left(\frac{1}{4}\varphi^4 - \frac{1}{2}\left(\frac{v_0}{v}\right)^2\varphi^2\right) - \frac{g_3(T)^2}{12\pi}\left(\frac{3}{8}\varphi^3 + 3\left[\frac{1}{4}\varphi^2 + \frac{\lambda_T}{g^2}\left(\varphi^2 - \left(\frac{v_0}{v}\right)^2\right)\right]^{3/2}\right) \quad (2.25)$$

and the Z-function

$$Z_H(\varphi) = 1 + \frac{g_3(T)^2}{4\pi}\left[-\frac{3}{m_W + m_\chi} + \frac{3}{64}\frac{1}{m_W^3}\varphi^2 - \frac{2}{64}\frac{1}{m_{\rm gh}^3}\varphi^2 + \frac{1}{64}\frac{1}{m_\chi^3}\left(1 + 4\frac{\lambda_T}{g^2}\right)^2\varphi^2\right] . \quad (2.26)$$

The effective potential predicts a first-order phase transition. (We are restricting ourselves to zero-temperature Higgs masses $\tilde{m}_H \leq \tilde{m}_W$.) In the transition range it has two minima, the symmetric one at $\varphi_S = 0$ and the asymmetric one at $\varphi_A = v(T)$. During the phase transition φ takes on values between φ_S and φ_A. The most natural way of rescaling the field in eq. (2.1) is therefore to choose $v = v(T)$. Hence the asymmetric minimum is always at $\varphi_A = 1$.

The parameter $\frac{v_0(T)^2}{v(T)^2}$ introduces the temperature dependence into the potential. The effective coupling $g_3(T)$ is related to this parameter by the requirement that the minimum of the potential corresponding to the broken symmetry phase is located at $\varphi_A = 1$, according to the field rescaling. The critical temperature T_c corresponds to the two minima having equal height. At the roll-over temperature $T_{\rm ro}$ the symmetric phase becomes unstable. In figure 1 we show $\frac{v_0(T)^2}{v(T)^2}$ as function of $\frac{\lambda_T}{g^2}$, for $T = T_c$ and $T = T_{\rm ro}$, respectively. $g_3(T)^2$ at $T = T_c$ and $T = T_{\rm ro}$ is shown in figure 2 .

2.4 The gauge-fixing dependence of the effective action

The effective potential (eq. (2.25)) is not a polynomial in φ, due to the non-vanishing $\frac{\lambda_T}{g^2}$-term of the Goldstone mass (eq. (2.25)). Nevertheless, the corrections induced by this term are (at least for $\tilde{m}_H \leq \tilde{m}_W$) numerically small. They manifest themselves in three (small) effects:
i) The critical temperature T_c and the roll-over temperature $T_{\rm ro}$ are shifted towards higher temperatures.
ii) $V_{\rm eff}(\varphi = 0)$ is shifted. This is corrected by adding a constant to the potential. We always work with $V_{\rm eff}(0) = 0$.
iii) The effective Higgs mass defined by $\sqrt{V''_{\rm eff}(\varphi)}$ has different values in the symmetric and in the asymmetric phase. (cf. our note on the Higgs masses in section 3.3)

Note that the contribution from the $\frac{\lambda_T}{g^2}$-term of the Goldstone mass is the only gauge-dependent part of $V_{\rm eff}(\varphi)$. Integrating out gauge bosons, Goldstones and ghosts in the limit of vanishing $\frac{\lambda_T}{g^2}$ the effective potential is independent of the gauge parameter ξ. The gauge-fixing dependent contributions due to the non-vanishing $\frac{\lambda_T}{g^2}$ are numerically small.

The situation is totally different looking at the Z-function (eq. (2.26)). Comparing our results with those obtained in Landau gauge (see e.g. [3]) the contribution from the mixed W-χ loops get a factor $\frac{2}{3}$ while the sum of the W and the ghost loops which has to be taken as one part gets a factor 10. The χ-loop contribution is the same.

In figure 3 we have plotted the Z_H-function at the critical temperature in 't Hooft-Feynman as well as in Landau gauge. The results are totally different. Note that this strong gauge-fixing dependence can not be cured by introducing a magnetic mass of any reasonable size. In the spirit of ref. [14] one might argue that the gauge-fixing dependence of Z_H in one-loop order cancels against the gauge-fixing dependence of V_{eff} in two-loop order. Indeed in the thin-wall limit, for $\frac{\lambda_T}{g^2} \to 0$, one can see explicitly that higher derivative terms compete with lower derivative higher loop terms evaluated in the critical bubble background. Away from this limits, however, we expect that also a cancellation against higher derivative terms of the same loop order plays an important role.

2.5 Limits on derivative expansion and perturbation theory

In calculating S_{eff} we have integrated out the gauge and Goldstone degrees of freedom well separated from the Higgs field φ in one-loop order. In the range of small φ these are massless or light modes and one has to be aware of the breakdown of derivative expansion: the true effective action is a non-local functional of φ. Indeed if one calculates higher derivative terms (beyond $(\partial\varphi)^2$) the singularities of the higher order Z-factors get worse. If one inserts the critical bubble solutions obtained with the usual kinetic term (and to be discussed in section 3.2) into the effective action functional stated in derivative expansion these terms diverge contrary to the $\int d^3x Z(\varphi)(\partial\varphi)^2$ term. The latter term, however, has defects as well. As mentioned above it is highly gauge-dependent and $Z(\varphi)$ also turns out to become negative in some φ-range in t' Hooft-Feynman gauge. This makes it impossible to use the effective action resulting from the derivative expansion for a further treatment of the η fluctuations.

As an alternative to the derivative expansion, one may perform a heat kernel expansion. This is also a local expansion, but instead of summing contributions of a given number of derivatives to all orders, terms with different number of derivatives are systematically combined order by order. In this way, more and more non-locality is covered. There is no obvious scale and therefore the dynamics of the symmetric phase is plagued by infrared problems. However, what we really want to know is a difference of the bubble effective action to the effective action of the symmetric phase. The bubble solution provides additional scales which may serve as infrared cut-off. As mentioned above (section 2.2) this scale is set by the inverse bubble wall thickness and turns out to be rather small. Therefore, the heat kernel expansion may converge reasonably well also in the presence of massless modes. This will not be attempted in this paper.

In order to take non-local effects into account in some approximate way, we shall introduce some φ independent wave-function renormalization for the kinetic term of the Higgs field

$$S_z[\varphi(\vec{x})] = \frac{1}{g_3(T)^2} \int d^3x \left[\frac{1}{2} z (\partial_i \varphi)^2 + V_{\text{eff}}(\varphi(\vec{x})) \right] \quad . \tag{2.27}$$

z would have to be determined from the true non-local effective action in such a way that $S_z[\varphi]$ approximates that action locally in some neighborhood of the critical bubble (but not globally in field space, which is not possible). Therefore, z is not directly related to the wave-function renormalization $Z_H(\varphi)$ (eq. (2.26)) but also summarizes the effect of all the

higher derivative operators. Unfortunately, a fit of z is technically involved and presently not feasible. One should insert trial functions extremizing eq. (2.27) into the higher order heat kernel expansion containing the 12×12 matrix potential. In the resulting terms the z-dependence factorizes out, and the total expression should be extremized with respect to z.

One could also try to find some average $z_{\rm av}$ arguing that the small φ-range is not important in the integrated action at least for small $\tilde{m}_H$. In view of the negative $Z(\varphi)$-range we are sceptical about this procedure. Nevertheless we will present a plot of such a $z_{\rm av}$ in section 3.2.

Note that the breakdown of the derivative expansion does not automatically imply the breakdown of perturbation theory. To inspect the latter question we calculated (Appendix A) the $Z_{\rm gauge}(\varphi)$ prefactor of the gauge-kinetic term in one-loop order. This term does not appear directly in the Higgs Lagrangian but $g_3(T)^2/Z_{\rm gauge}(\varphi)$ is the effective gauge coupling at the scale φ. Figure 4 demonstrates that it becomes big (Z small or negative, respectively) already halfway in φ between the broken and unbroken minimum even for small $\tilde{m}_H$ ($\tilde{m}_H = \frac{1}{2}\tilde{m}_W$). This means that the perturbative expansion breaks down in a rather big range of φ starting from $\varphi = 0$, and that we cannot trust the perturbative potential and action for these Higgs field values φ. This was already emphasized in ref. [15]. It is not clear, however, at what effective scale the gauge coupling will appear in higher loop order. Nevertheless, one has to expect a rather strong dependence of the bubble solutions on this part of the action (different from sphaleron configurations based on the broken phase [16]), Also the potential in the ansatz eq. (2.27) might get nonperturbative contributions. They are not considered in this paper.

3 The Phase Transition

3.1 Nucleation rate

According to the effective action calculated above the electroweak phase transition is of first-order. It is triggered by bubble nucleation. Just before the transition starts the system is in thermal equilibrium in the metastable symmetric phase.

The onset of a first-order phase transition was investigated by Langer [7] and successive work [17, 18] in some detail. The bubble nucleation at the electroweak phase transition has been investigated e.g. in the references [19] and [20]. It is assumed that the total system is dividable into interval and system of interest [21]. The influence of the heat bath on the rest is first to induce thermal fluctuations and second to change the free energy of the system of interest. Both influences are only taken into account on average. We divide the total system, which consists of all fields of the standard model, into the ω_0-frequency of the real scalar field $\varphi = \sqrt{2\Phi^\dagger\Phi}$ and the rest. The free energy is given by $\beta F[\varphi(\vec{x})] = S[\varphi(\vec{x})]$ where $S[\varphi(\vec{x})]$ is the effective action.

Langer solved the equations of motion in a neighborhood of the saddlepoint, which corresponds to the critical bubble, and got a quasi-stationary solution describing a density flow from the metastable to the stable region. The transition rate Γ is the integral of density flow and evaluates to

$$\Gamma = \frac{\kappa}{2\pi} V \left(\frac{\bar{S}}{2\pi}\right)^{3/2} \frac{1}{\sqrt{|\lambda_-|}} \left[\frac{\det'' K}{\det K_0}\right]^{-1/2} \exp\{-\bar{S}\} \tag{3.1}$$

where

- κ is the dynamical prefactor. It takes into account the dynamical characteristics of the heat bath. We will not calculate it in this paper but refer to the literature [22].
- V is the spatial volume.
- $$K = g_3(T)^2 \frac{\delta^2 S}{\delta \varphi^2}\Big|_{\bar{\varphi}(\vec{x})} \qquad K_0 = g_3(T)^2 \frac{\delta^2 S}{\delta \varphi^2}\Big|_{\varphi_s} \tag{3.2}$$

  $\bar{\varphi}(\vec{x})$ is the critical bubble and φ_s represents the symmetric phase. $\det{}'' K$ denotes the determinant of K, without the negative and the three zero eigenvalues. The negative eigenvalue corresponds to the growing and shrinking of the critical bubble. The zero-modes are due to translational invariance. The factors $g_3(T)^2$ result from a rescaling which makes formulas more convenient.
- λ_- is the negative eigenvalue of K.
- $\bar{S} = S[\bar{\varphi}(\vec{x})] - S[\varphi_s]$ is the effective action of the critical bubble.

$\bar{S}, \lambda_-$ and the static prefactor

$$A = \left[\frac{\det{}'' K}{\det K_0}\right]^{-1/2} \tag{3.3}$$

are functionals of the critical bubble $\bar{\varphi}(\vec{x})$. The latter depends only on the temperature. The determinants now refer to the Higgs field fluctuations only.

One aim of our work is to calculate the rate

$$R = \frac{\Gamma}{V\kappa} = \frac{1}{2\pi}\left(\frac{\bar{S}}{2\pi}\right)^{3/2} \frac{1}{\sqrt{|\lambda_-|}} A \exp\{-\bar{S}\} \tag{3.4}$$

as a function of the temperature.

We will describe our calculation for the zero-temperature Higgs mass $\tilde{m}_H = \frac{1}{2}\tilde{m}_W$ in some detail and report the results for other values of $\tilde{m}_H$ at the end.

3.2 The critical bubble

The critical bubble $\varphi(\vec{x})$ is a saddlepoint of the effective action $S[\varphi]$ and therefore a solution of

$$\frac{\delta S}{\delta \varphi}\Big|_{\bar{\varphi}(\vec{x})} = 0 \tag{3.5}$$

with the boundary conditions

$$\lim_{\vec{x}\to\infty} \bar{\varphi}(\vec{x}) = \varphi_S \qquad \bar{\varphi}(0) > \varphi_S \quad . \tag{3.6}$$

Taking the effective action $S_z[\varphi]$ the saddlepoint equation reads

$$z\partial^2 \bar{\varphi}_z(\vec{x}) - V'_{\text{eff}}(\bar{\varphi}_z(\vec{x})) = 0 \quad . \tag{3.7}$$

By rescaling $\vec{x} \to \vec{x}/\sqrt{z}$ this equation reduces to the one with $z = 1$. The solution for arbitrary but constant $z > 0$ is therefore

$$\bar{\varphi}_z(\vec{x}) = \bar{\varphi}\left(\frac{\vec{x}}{\sqrt{z}}\right) \qquad \text{with} \qquad \bar{\varphi} = \bar{\varphi}_{z=1} \quad . \tag{3.8}$$

To cover the whole temperature range from the new roll-over temperature $T_{\rm ro}$ to the critical temperature T_c we introduce a temperature-like variable y instead of $\frac{v_0(T)^2}{v(T)^2}$ via

$$\left(\frac{v_0(T)^2}{v(T)^2}\right)_y = \frac{v_0(T_c)^2}{v(T_c)^2} + y\left(\frac{v_0(T_{\rm ro})^2}{v(T_{\rm ro})^2} - \frac{v_0(T_c)^2}{v(T_c)^2}\right)$$

$$y = 0.1, 0.2, \ldots, 0.9 \quad . \tag{3.9}$$

This way of dividing the interesting temperature interval turned out to be much more appropriate than dividing it into equal ΔT intervals. For a given value of y the temperature T and the effective action (eq. (2.27)) are determined; the temperatures are given in table 1. We have calculated the critical bubbles from eq. (3.7) with $z = 1$ for these nine y's; they are spherical symmetric and plotted in figure 5.

The effective action of the critical bubble with arbitrary $z > 0$ is, using eq. (3.8)

$$\begin{aligned} {\rm S}_z[\bar\varphi_z] &= \frac{1}{g_3(T)^2}\int d^3x \left[\frac{1}{2}z\left(\partial_i\bar\varphi_z(\vec x)\right)^2 + V_{\rm eff}(\bar\varphi_z(\vec x))\right] \\ &= z^{3/2} \quad S_1[\bar\varphi(\vec x)] \end{aligned} \tag{3.10}$$

with

$$S_1[\bar\varphi(\vec x)] = \frac{1}{g_3(T)^2}\int d^3x \left[\frac{1}{2}(\partial_i\bar\varphi(\vec x))^2 + V_{\rm eff}(\bar\varphi(\vec x))\right] \quad . \tag{3.11}$$

This simple scaling behavior clarifies the roll of the corrections to the surface term and allows to proceed without knowing the value of z precisely.

Assuming that $V_{\rm eff}$ is renormalized by $V_{\rm eff}(0) = 0$ we identify $\bar S$ with $S_1[\bar\varphi]$. It is given in table 1 and plotted in figure 9 where single points are connected by a spline (full line).

With a known critical bubble configuration one can evaluate

$$z_{\rm av} = \frac{\int d^3x Z(\bar\varphi_z)(\partial\bar\varphi_z)^2}{\int d^3x(\partial\bar\varphi_z)^2} = \frac{\int d^3x Z(\bar\varphi)(\partial\bar\varphi)^2}{\int d^3x(\partial\bar\varphi)^2} \tag{3.12}$$

in order to get an average $z_{\rm av}$. In figure 6 we have plotted it for $\tilde m_H = \frac{1}{2}\tilde m_W$ versus y. However, in our opinion the range near $\varphi = 0$ is not taken into account properly in this way, because $Z(\varphi)$ is unphysical, as argued in section 2.5.

3.3 Eigenvalues of K and K_0

Using the effective action $S_z[\varphi]$ (eq. (2.27)) the operators K and K_0 defined in eq. (3.2) are

$$K = -z\partial^2 + U \qquad U = V''_{\rm eff}(\bar\varphi_z(r)) \tag{3.13}$$

$$K_0 = -z\partial^2 + U_0 \qquad U_0 = V''_{\rm eff}(\varphi_S) = m_H(T)^2 \quad . \tag{3.14}$$

U_0 is the squared effective mass of the Higgs field in the symmetric phase and the natural mass-scale of the remaining effective action.

Note that there is a change in notation. U and U_0 are in this chapter no matrices as in eq. (2.15) but real-valued functions of φ. The Higgs mass in eq. (2.16) corresponds to the high-temperature action (eq. (2.2)). It is φ and, via $\frac{v_0}{v}$, temperature-dependent. $m_H(T)$ defined in eq. (3.14) corresponds the effective action of eq. (2.27). It is the effective Higgs mass in the symmetric phase (i.e. at φ_S) and hence only temperature dependent.

In principle it is possible to define a φ-dependent effective Higgs mass via $m_H(T,\varphi)^2 = V''_{\rm eff}(\varphi)$, but this squared mass is negative for some φ-values. We do not need it.

The negative eigenvalue of K is determined by the eigenvalue equation

$$K\, n(\vec{x}) = (-z\partial^2 + V''(\bar{\varphi}_z(\vec{x}))\, n(\vec{x}) = \lambda_-\, n(\vec{x}) \quad . \tag{3.15}$$

By rescaling $\vec{x} \to \sqrt{z}\vec{x}$ and using eq. (3.8) one sees that λ_- is independent of z. Similarly all other eigenvalues of K and K_0 are z-independent. We calculated λ_- numerically by solving the Schrödinger equation (3.15) with the boundary condition

$$\lim_{r\to\infty} n(r) = 0 \quad . \tag{3.16}$$

The static prefactor A (eq. (3.3)) is a product of eigenvalues of K and K_0 and therefore independent of z. We evaluate it for $z = 1$.

3.4 Heat-kernel method and calculation of the static prefactor

Starting from

$$\ln\left(\frac{\det K}{\det K_0}\right) = -\mathrm{Tr}\int_0^\infty \frac{dt}{t} e^{-at}\left(e^{-t(K-a)} - e^{-t(K_0-a)}\right) \tag{3.17}$$

it is possible to expand the logarithm in power of t [23]. A very elegant method to do this is provided by a new calculation scheme [9]. One gets

$$\begin{aligned}\ln\left(\frac{\det K}{\det K_0}\right) &= -\sum_{n=1}^\infty \frac{1}{n!}\int_0^\infty \frac{dt}{t}(4\pi t)^{-3/2} e^{-at} t^n (O_n(a) - O_n^{(0)}(a)) \\ &= -\sum_{n=1}^\infty \frac{\Gamma(n-3/2)}{n!}(4\pi)^{-3/2} a^{3/2-n}(O_n(a) - O_n^{(0)}(a)) \quad . \end{aligned} \tag{3.18}$$

The $O_n(a)$'s and $O_n^{(0)}(a)$'s are rather complicated functionals of $\bar{\varphi}(\vec{x})$ which are given in Appendix C. They depend on the mass scale a pulled out in eq. (3.17). In doing the t-integration for $n = 1$ we have dimensionally regularized the UV-divergence which may be traced back to the reduction in dimension [24]. Note that pulling out the squared mass a in eq. (3.17) regularizes the IR-divergencies and makes the t-integral finite at the upper bound. This is an advantage over the method proposed in ref. [25].

However eq. (3.17) is only valid for positive definite K and K_0. In our case, K has one negative and three zero-eigenvalues. Exactly these eigenvalues are left out of the static prefactor (eq. (3.3)) of the nucleation rate anyway. On the other hand, we have to drop four eigenvalues of K_0 as well, if we want to use eq. (3.17), because this equation makes use of the fact that the numbers of eigenvalues of K and K_0 are equal.

Taking out four times the eigenvalue U_0 from $\det K_0$ one gets

$$\begin{aligned}&\ln\left(U_0^4\frac{\det'' K}{\det K_0}\right) = \ln\left(\frac{\det'' K}{\det'' K_0}\right) \\ &= \int_0^\infty \frac{dt}{t}\left[-\left(\mathrm{Tr}\left\{e^{-tK}\right\} - e^{-t\lambda_-} - 3\right) + \left(\mathrm{Tr}\left\{e^{-tK_0}\right\} - 4e^{-tU_0}\right)\right] \\ &= \int_0^\infty \frac{dt}{t} e^{-at}\left[-\mathrm{Tr}\left\{e^{-t(K-a)} - e^{-t(K_0-a)}\right\} + \right.\end{aligned}$$

$$+\left(e^{-t(\lambda_- - a)} - e^{-t(U_0-a)}\right) + 3\left(e^{at} - e^{-t(U_0-a)}\right)\Big]$$

$$= \int_0^\infty \frac{dt}{t} e^{-at}\left[-\sum_{n=1}^{\infty}\frac{1}{n!}(4\pi)^{-3/2}t^{n-3/2}\left(O_n(a) - O_n^{(0)}(a)\right) + \right. \tag{3.19}$$

$$\left. + \sum_{n=1}^{\infty}\frac{1}{n!}t^n\left((a-\lambda_-)^n - (a-U_0)^n\right) + 3\sum_{n=1}^{\infty}\frac{1}{n!}t^n\left(a^n - (a-U_0)^n\right)\right] \quad .$$

From the sum over the O's only the first few terms are calculable. Therefore we have to truncate the other two sums as well. From similar calculations with other models we found that the truncation is best done at the 'same' powers of t rather than at the same number N of terms (see also [26, 27]). This cannot be done straightforwardly however, because the O-sum runs over half-integer power of t while the other sums run over full-integer powers. We solved the problem by defining the two functions

$$X(N,a) = \int_0^\infty \frac{dt}{t} e^{-at}\left[-\sum_{n=1}^{N}\frac{1}{n!}(4\pi)^{-3/2}t^{n-3/2}\left(O_n(a) - O_n^{(0)}(a)\right)\right]$$

$$= -\sum_{n=1}^{N}\frac{\Gamma(n-3/2)}{n!}(4\pi)^{-3/2}a^{3/2-n}\left(O_n(a) - O_n^{(0)}(a)\right) \tag{3.20}$$

and

$$Y(N',a) = \int_0^\infty \frac{dt}{t} e^{-at}\sum_{n=1}^{N'}\frac{1}{n!}t^n\left((a-\lambda_-)^n + 3a^n - 4(a-U_0)^n\right)$$

$$= \sum_{n=1}^{N'}\frac{1}{n}\left[\left(\frac{a-\lambda_-}{a}\right)^n + 3 - 4\left(\frac{a-U_0}{a}\right)^n\right] \quad . \tag{3.21}$$

While we have been able to evaluate $X(N,a)$ for $N \in \{1,2,3,4,5,6\}$ [3], $Y(N',a)$ could be calculated for every integer N'. We interpolated $Y(N',a)$ by a spline and defined the functions

$$W_N(a) = X(N,a) + Y(N - \frac{3}{2}, a) \quad . \tag{3.22}$$

From the equations (3.3, 3.19 – 3.22)

$$\lim_{N\to\infty} W_N(a) = \ln\left(U_0^4 \frac{\det{}'' K}{\det K_0}\right) = -2\ln\left(\frac{A}{m_H(T)^4}\right) \tag{3.23}$$

follows. While the $W_N(a)$'s are functions of a, the limit is not. This will give us a good criterion for the quality of convergence [21].

For every critical bubble calculated above we have evaluated the functions $W_1(a), \ldots, W_6(a)$. Figure 7 shows the typical behavior. If a – the squared mass pulled out – is too small, there is no convergence at all. If a is too big, the convergence is bad. But if a is similar to the natural mass scale U_0, the functions converge quite well towards a constant, which is plotted as dashed line.

There are several sources of error in the outlined procedure: numerical errors, ambiguities in interpolating $Y(N',a)$ and uncertainties in fixing the limit of the $W_N(a)$'s. We have estimated them to be less than 2% . The values of $\ln(A/T^4)$ are listed in table 1 and plotted in figure 9 (dashed line).

[3] One could evaluate $X(7,a)$ as well [9], but this does not appear necessary in view of the excellent convergence.

3.5 The static prefactor and the effective action of the critical bubble

Up to now the static prefactor has usually been estimated from dimensional reasons as T^4 [18], or as $m_H(T)^4$ [20]. There are some other calculations of the prefactor, which take only into account the lowest eigenvalues of K [28, 29]. The results of these calculations are somewhere between the two dimensional estimates. To compare our results with these values we have expressed A in units of GeV. In figure 8 they are plotted together with these two estimates. One sees that the static prefactor calculated by us varies substantially from $y = 0.1$ to $y = 0.9$. On the side of the critical temperature ($y = 0$) it is much smaller than previous values. This results in a much smaller nucleation rate.

In a recent paper [30] the fluctuation corrections to critical bubbles calculated from the usual model effective potential are discussed. The method is based on the solution of Schrödinger type eigenvalue equations and totally different from our procedure. Unfortunately the present results are hard to compare because in ref. [30] the high-temperature limit is not taken and because the potential differs in detail. A comparison of the two methods in a common case would be very interesting.

The logarithm of the rate R/T^3 defined in eq. (3.4) is

$$\ln\left(\frac{R}{T^3}\right) = \ln\left(\frac{1}{2\pi}\left(\frac{\bar{S}}{2\pi}\right)^{3/2}\frac{T}{\sqrt{|\lambda_-|}}\right) + \ln\left(\frac{A}{T^4}\right) - \bar{S} \quad . \tag{3.24}$$

The different contributions are plotted in comparison in figure 9. One sees that the first one is small and nearly constant. The nucleation rate is determined by $-\bar{S}$ and $\ln(A/T^4)$. The comparison of these two values decides on the reliability of our results. $-\ln(A/T^4)$ is nothing but the one-loop correction to $\bar{S}$ coming from scalar loops. Therefore $|\ln(A/T^4)| \ll \bar{S}$ is required for consistency.

Very close to the critical and the roll-over temperature it matters that the radiative corrections shift the values of T_c and $T_{\rm ro}$. This effect should perhaps better be incorporated in the quasiclassical effective action. In our approach it causes an increase of the static prefactor near these temperatures. However, investigating the electroweak phase transition the interesting temperatures are well separated from T_c and $T_{\rm ro}$, as we will see below.

In Langer's theory the static prefactor A takes the possibility into account that the phase transition may be started by a bubble which differs from the critical one. On the other hand the whole theory is based on a solution of the equations of motion in the neighborhood of the saddlepoint that corresponds to the critical bubble. From this reasoning one again gets that $|\ln(A/T^4)| \ll \bar{S}$ should be valid. This comparison is not unambiguous because $\bar{S}$ is dimensionless while A is not. Expressing A in T seems to be appropriate because the temperature is the typical scale of the phase transition.

Therefore the nucleation rate calculated by us is not reliable at temperatures near the roll-over temperature $y = 1$. Taking estimates based on cosmological reasons however, the electroweak phase transition starts when $\ln(R/T^3) \approx 140$. [4] The relative starting temperature is therefore $y_s = 0.42$. At this temperature $|\ln(A/T^4)| \approx 0.3\bar{S}$. This is an acceptable correction.

However, with z smaller than 1 we find according to eq. (3.10) an additional suppression of the leading term ($\bar{S}$), i.e. the the one-loop contribution becomes relatively more important, indicating a less convergent loop expansion.

[4] Here we have assumed that $\kappa = \mathcal{O}(1)$.

3.6 Results for other Higgs masses

The numerical calculations presented have been done for the zero temperature Higgs masses $\tilde{m}_H = \frac{1}{2}\tilde{m}_W, \frac{3}{4}\tilde{m}_W$ and $\tilde{m}_W$. The results are listed in the tables 1, 2 and 3.

The critical temperature T_c and the roll-over temperature $T_{\rm ro}$ depend on the Higgs mass. One should compare values corresponding to different masses at the same relative temperature y defined in eq. (3.9). The actions $\bar{S}$ of the critical bubbles depend strongly on the Higgs mass, while the Higgs mass dependence of the static prefactor is only small. Although the rates are quite different for the three masses the relative onset temperatures differ only moderately. This is due to the fact that the rates decrease rapidly when the temperature is lowered.

We have listed the relative onset temperatures in table 4 together with the corresponding values of $\bar{S}$, $\ln(A/T^4)$ and the quotient of both. This quotient decides, as argued above, on the reliability of the nucleation rate formula (eq. (3.1)). One sees that the corrections get worse if the Higgs mass increases.

3.7 Comparison with the thin-wall approximation

If the temperature is just below the critical temperature T_c the radius R of the critical bubble is much larger than the size of the bubble wall ΔR. In the limit $T \to T_c$ and $\Delta R \ll R$ the effective action of the critical bubble can be written as (for $z = 1$)

$$\bar{S}_{\rm TW} = \frac{1}{g_3^2}\frac{16\pi\sigma^3}{3\epsilon^2} \tag{3.25}$$

with the volume energy

$$\epsilon = -V_{\rm eff}(T, \varphi_A) \tag{3.26}$$

and the surface tension

$$\sigma = \int_{\varphi_S}^{\varphi_A} d\varphi \sqrt{2V_{\rm eff}(T_c, \varphi(r))} \tag{3.27}$$

(cf. appendix B). The values of σ are given in table 5. The values of $\bar{S}_{\rm TW}$ are listed in comparison with the full numerical values of the critical bubbles effective actions. (See figure 10 as well.) The shape of the critical bubbles is far from thin-wall except in the case $y = 0.1$ (cf. figure 5, for other Higgs masses the bubbles are similar). Nevertheless the thin-wall estimates of the corresponding effective actions are quite good even for smaller temperatures. On the other hand one has to calculate the critical bubble configurations themselves if one wants to evaluate the static prefactor.

4 Discussion and Conclusions

Our main result is a very accurate determination of the Higgs fluctuation determinant for critical bubble solutions for an action (eq. (2.27)). It leads to a rather drastic change in the prefactor A of the transition rate compared to previous rough estimates as indicated in figure 8. The transition is suppressed stronger. It is interesting to note that the radiative corrections do not depend on the normalization factor z while the quasiclassical bubble action scales with $z^{3/2}$. In our procedure to evaluate the heat kernel expansion it was essential that we go to a rather high order, that we take out a variable scale and that we treat the subtraction of the unstable and zero modes carefully. The separate interpolation

for integer and half integer O_n before the subtraction is essential for the quality of the approximation.

We have also discussed the critical bubble configurations and their action for various temperatures between T_c and $T_{\rm ro}$, and Higgs masses. For $\tilde{m}_H \leq \frac{3}{4}\tilde{m}_W$ and temperatures not too close to $T_{\rm ro}$ the radiative corrections are small compared to the $z = 1$ quasiclassical action term (see table 2). Surprisingly the thin-wall approximation for the action is quite good at temperatures where the critical bubble profile is not 'thin-wall' any more. The dependence of the action on the constant Z-factor can be taken out explicitly. It is an interesting side remark that the usual thin-wall machinery goes through even for arbitrary positive factors $Z(\varphi)$ (Appendix B).

In the first part of the paper we discussed the status of a perturbative effective Higgs action. The 't Hooft-Feynman covariant background gauge is particularly well suited for a discussion of the separate integration of gauge, Goldstone, and ghost fields, and also avoids IR problems near the broken phase vacuum. The size of the rescaled 3-dimensional gauge coupling $g_3(T)^2$ in the broken phase changes smoothly in the phase transition and is not very big and not very small; thus both the perturbative expansion in g_3^2 and the high temperature expansion seem to work. The inspection of the one-loop Z prefactors of the Higgs and gauge-kinetic terms tells us however, that this is only true in the broken phase.

Even at small $\tilde{m}_H \sim \frac{1}{2}\tilde{m}_W$ the Higgs $Z_H(\varphi)$ (figure 3) becomes negative already at rather big values of φ of the Higgs fields in our gauge. Different from the one-loop potential, $Z_H(\varphi)$ is very gauge-dependent and differs from the Landau gauge. The negativity of Z_H cannot be changed by the introduction of a reasonable magnetic mass. The latter can only change the singular behavior of $Z_H(\varphi)$ for φ very close to zero. As we argued in chapter 3, this signals the breakdown of the derivative expansion.

Even worse, the gauge field $Z_{\rm gauge}(\varphi)$ becomes negative at still larger values of φ. Since it gives the static φ-dependent effective gauge coupling[5] $g_3(T)^2/Z_{\rm gauge}(\varphi)$, this signals the breakdown of perturbation theory for a big range of φ already at small $\tilde{m}_H \sim \frac{1}{2}\tilde{m}_W$ (figure 4), though the optimal choice of a scale of a gauge coupling in multi-loop calculations in the background of a critical bubble is not known. Thus, the use of a Higgs action (eq. (2.27)) inspired by perturbation theory in the discussion of the critical bubbles does not have a firm ground. The 'small' φ region contributes directly to the critical bubble action through the Higgs kinetic term and not so much through the potential, but of course there is an indirect effect of the potential changing (perhaps drastically) the critical bubble configuration itself.

Acknowledgments

We would like to thank W. Buchmüller and C. Wetterich for useful discussions.

[5] We have checked that this behavior gives the bound $\frac{m_W(T,\varphi)}{T} > 0.1$ for a perturbative treatment to be compared with $\frac{m_W(T,\varphi)}{T} > 0.2$ from a renormalization group calculation [31].

Appendix A: Calculation of the Wave Function Renormalization Z Factors

In this Appendix we calculate the Z factors in front of the kinetic terms. We work in 't Hooft-Feynman background gauge (eq. (2.9)).

We first assume that there is only a real scalar background field (eq. (2.8)). The task is to expand δS (eq. (2.21)) in powers of $\partial\varphi$. It reduces to the calculation of

$$W = \log\det(-\partial^2 + U) = \frac{1}{3}\log\det(-\partial^2 + M_{12}) \tag{A.1}$$

where U is given in eq. (2.14). Following [13] we expand

$$W = \int \frac{d^3k}{(2\pi)^3}\left[\int d^3x \mathrm{tr}\log(\Delta^{-1}) + \frac{k^2}{3}\int d^3x \mathrm{tr}(\partial_i\Delta)^2 + \dots\right] \tag{A.2}$$

where

$$\Delta = (k^2 + U(\varphi(\vec{x}))^{-1} \quad . \tag{A.3}$$

tr denotes the trace over the 4×4-matrices. The logarithm is expanded as

$$\begin{aligned}\mathrm{tr}\log(\Delta^{-1}) &= \mathrm{tr}\log(k^2 + U_0 + \delta U)\\ &= \mathrm{tr}\log\left(\Delta_0^{-1}(1 + \Delta_0\delta U)\right)\\ &= \mathrm{tr}\left[\log(\Delta_0^{-1}) + \sum_{n=1}^{\infty}\frac{(-1)^n}{n}(\Delta_0\delta U)^n\right]\end{aligned} \tag{A.4}$$

where U_0 and δU are given in eq. (2.15) and

$$\Delta_0 = (k^2 + U_0)^{-1} = \begin{pmatrix} (k^2+m_W^2)^{-1} & 0 & 0 & 0\\ 0 & (k^2+m_W^2)^{-1} & 0 & 0\\ 0 & 0 & (k^2+m_W^2)^{-1} & 0\\ 0 & 0 & 0 & (k^2+m_\chi^2)^{-1}\end{pmatrix} \tag{A.5}$$

Calculating the Z-function only the terms proportional to $(\partial\varphi)^2$ are of interest. Hence only the $n=2$ term contributes, and the relevant part of the first term on the r.h.s. of eq. (A.2) is

$$\begin{aligned}&\int\frac{d^3k}{(2\pi)^3}\int d^3x\frac{1}{2}\mathrm{tr}(\Delta_0\delta U\Delta_0\delta U)\\ =\ &\int\frac{d^3k}{(2\pi)^3}\int d^3x\frac{1}{k^2+m_W^2}\frac{1}{k^2+m_\chi^2}(\partial_i\varphi)^2\\ =\ &\int d^3x\frac{1}{4\pi}\frac{1}{m_W+m_\chi}(\partial_i\varphi)^2 \quad .\end{aligned} \tag{A.6}$$

To evaluate the second term on the r.h.s. of eq. (A.2) we make use of the fact that

$$\Delta = \Delta_0 + \mathcal{O}(\partial\varphi) \quad . \tag{A.7}$$

Since we are only interested in terms proportional to $(\partial\varphi)^2$ we may replace Δ by Δ_0. The latter is diagonal and the trace tr reduces to a sum over the field degrees of freedom. For

one degree one gets

$$\begin{aligned}
&\int \frac{d^3k}{(2\pi)^3}\frac{k^2}{3}\int d^3x(\partial_i(k^2+m^2)^{-1})^2 \\
= &\int d^3x\frac{1}{3}\int\frac{dk}{(2\pi)^3}\left(\frac{-k^2}{(k^2+m^2)^2}\left(\frac{\partial m^2}{\partial\varphi}\right)\partial_i\varphi\right)^2 \\
= &\int d^3x\frac{1}{192\pi}\frac{1}{m^3}\left(\frac{\partial m^2}{\partial\varphi}\right)^2(\partial_i\varphi)^2 \quad . \qquad \text{(A.8)}
\end{aligned}$$

The ghost calculation is exactly the same (cf. eq. (2.21) and eq. (2.22)).

Finally one has to put the parts together and get the factors right. Eq. (A.8) has to be summed over 9 gauge fields components, 3 Goldstones and 3 ghosts. Eq. (A.6) has to be multiplied by 3 from eq. (A.1). From eq. (2.21) one gets a factor $\frac{1}{2}$ respectively -1. The result is

$$\begin{aligned}
\int d^3x\,\frac{1}{2}\,\Bigg[&-\frac{3}{4\pi}\frac{1}{m_W+m_\chi}+\frac{3}{64\pi}\frac{1}{m_W^3}\left(\frac{\partial m_W^2}{\partial\varphi}\right)^2 \\
&-\frac{2}{64\pi}\frac{1}{m_{\rm gh}^3}\left(\frac{\partial m_{\rm gh}^2}{\partial\varphi}\right)^2+\frac{1}{64\pi}\frac{1}{m_\chi^3}\left(\frac{\partial m_\chi^2}{\partial\varphi}\right)^2\Bigg](\partial_i\varphi)^2 \quad . \qquad \text{(A.9)}
\end{aligned}$$

Taking into account the factor $\frac{1}{2g_3^2}$ of eq. (2.23) one gets $Z_H(\varphi)$ (eq. (2.26)).

Integrating out the Higgs field as well, the effective potential (eq. (2.24)) gets an additional $-g_3(T)^2\frac{1}{12\pi}m_H^3$ term while the Z_H-factor (eq. (2.26)) is modified by

$$+\frac{1}{192\pi}g_3(T)^2\frac{1}{m_H^3}\left(\frac{\partial m_H^2}{\partial\varphi}\right)^2 \quad . \qquad \text{(A.10)}$$

With the complex scalar doublet and the gauge field as background fields the same method gives a Z-function in front of the kinetic Goldstone term

$$Z_\chi = 1-g_3(T)^2\frac{1}{24\pi}\left(\frac{\lambda}{g^2}-\frac{1}{8}\right)^2\varphi^2 m_\chi^{-3}-g_3(T)^2\frac{1}{4\pi}\left(\frac{2}{m_W+m_\chi}+\frac{1}{m_W+m_H}\right) \qquad \text{(A.11)}$$

and in front of $\frac{1}{4}F_{ij}^aF_{ij}^a$

$$Z_{\rm gauge} = 1-g_3(T)^2\frac{1}{8\pi}\left[\frac{7}{m_W}-\frac{1}{8m_\chi}-\frac{1}{24m_H}+\frac{1}{3m_{\rm gh}}\right] \quad . \qquad \text{(A.12)}$$

The logarithmic derivative of $Z_{\rm gauge}$ is the β-function of the theory. $Z_{\rm gauge}$ is plotted in figure 4 for $\tilde{m}_H=\frac{1}{2}\tilde{m}_W$, $\frac{3}{4}\tilde{m}_W$ and $\tilde{m}_W$ versus φ.

Appendix B: The Thin-Wall Approximation

If the extension ΔR of the bubble wall is small compared to the radius R of the critical bubble its effective action $S_1[\bar{\varphi}(r)]$ (eq. (3.11)) may be written as

$$\begin{aligned}
S_{\rm TW}[\bar{\varphi}(r)] &= \frac{1}{g_3(T)^2}4\pi\left[\int_0^{R-\Delta R/2}drr^2V(\bar{\varphi}(r))+\int_{R-\Delta R/2}^{R+\Delta R/2}drr^2\left[\frac{1}{2}(\partial_r\bar{\varphi}(r))^2+V(\bar{\varphi}(r))\right]\right] \\
&\approx \frac{1}{g_3(T)^2}\left[4\pi R^2\sigma-\frac{4\pi}{3}R^3\epsilon\right] \qquad \text{(B.1)}
\end{aligned}$$

with

$$\epsilon = -V(\varphi_A) \tag{B.2}$$

$$\sigma = \int_{R-\Delta R/2}^{R+\Delta R/2} dr \left[\frac{1}{2}(\partial_r \bar{\varphi}(r))^2 + V(\bar{\varphi}(r))\right] \quad . \tag{B.3}$$

In this appendix $V(\varphi)$ designates the effective potential. We assume that it is normalized by $V(0) = 0$.

Using $\Delta R \ll R$ again the saddlepoint equation (3.7) reads (z=1)

$$\frac{d^2\bar{\varphi}(r)}{dr^2} = V'(\bar{\varphi}(r)) \quad . \tag{B.4}$$

Solutions of this equation have the 'constant of motion'

$$\frac{1}{2}\left(\frac{d\bar{\varphi}(r)}{dr}\right)^2 - V(\bar{\varphi}(r)) \tag{B.5}$$

which is equal to $V(r \to \infty) = V(\varphi_S) = 0$ due to boundary conditions. Hence the surface tension may be written as

$$\sigma = \int_{\varphi_S}^{\varphi_A} d\varphi \sqrt{2V(\varphi(r))} \quad . \tag{B.6}$$

This integral is only real in the limit $T \to T_c$ where the derivation is exact.

Maximizing the thin-wall effective action with respect to the radius one gets the critical radius

$$R_c = \frac{2\sigma}{\epsilon} \tag{B.7}$$

and the effective action of the critical bubble as function of the surface tension σ and the volume energy ϵ

$$\bar{S}_{\rm TW} = \frac{1}{g_3^2}\frac{16\pi\sigma^3}{3\epsilon^2} \tag{B.8}$$

which has been evaluated in section 3.7 .

Using that $V(\varphi)$ scales with $\frac{\lambda_T}{g^2}$ in leading order one gets

$$\epsilon \propto \frac{\lambda_T}{g^2} \qquad \sigma \propto \left(\frac{\lambda_T}{g^2}\right)^{1/2} \qquad \bar{S}_{\rm TW} \propto \left(\frac{\lambda_T}{g^2}\right)^{-1/2} \quad . \tag{B.9}$$

The thin-wall approximation may even be done analytically for the effective action

$$S[\varphi(\vec{x})] = \frac{1}{g_3(T)^2}\int d^3x \left[\frac{1}{2}Z(\varphi)(\partial_i\varphi)^2 + V(\varphi(\vec{x}))\right] \tag{B.10}$$

with a general φ-dependent positive $Z(\varphi)$. The saddlepoint equation reads in this case

$$Z(\bar{\varphi})\partial^2\bar{\varphi} + \frac{Z'(\bar{\varphi})}{2}(\partial\bar{\varphi})^2 = V'(\bar{\varphi}) \quad . \tag{B.11}$$

With the substitution

$$V(\varphi) = \tilde{V}(\varphi)\cdot Z(\varphi) \tag{B.12}$$

we obtain

$$Z(\bar{\varphi})\partial^2\bar{\varphi} = Z(\bar{\varphi})\tilde{V}'(\bar{\varphi}) + Z'(\tilde{V}' - \frac{1}{2}(\partial\bar{\varphi})^2) \tag{B.13}$$

which is in thin-wall approximation solved by

$$\frac{d\bar{\varphi}}{dr} = \sqrt{2\tilde{V}(\bar{\varphi}(r))} \quad . \tag{B.14}$$

Repeating the steps from eq. (B.1) to eq. (B.8) but using this solution instead of eq. (B.5) we one may bring eq. (B.10) into the form eq. (B.8), but with

$$\sigma_Z = \int_{\varphi_S}^{\varphi_A} d\varphi \sqrt{2Z(\varphi)V(\varphi(r))} \tag{B.15}$$

instead of σ of eq. (B.6). For constant $Z(\varphi) = z$ this changes $S_{\rm TW}$ by a factor $z^{3/2}$ as it should according to eq. (3.10).

Appendix C: Operators of the Heat Kernel Expansion

The first six of the functionals $O_n(a)$ respectively $O_n^{(0)}(a)$ introduced in eq. (3.18) are [24, 9]

$$\begin{aligned}
O_1 &= \int dx\Big(U\Big) \\
O_2 &= \frac{1}{2!}\int dx\Big(U^2\Big) \\
O_3 &= \frac{1}{3!}\int dx\Big(U^3 + \frac{1}{2}\partial_\kappa U\partial_\kappa U\Big) \\
O_4 &= \frac{1}{4!}\int dx\Big(U^4 + 2U\partial_\kappa U\partial_\kappa U + \frac{1}{5}\partial_{\kappa\lambda}U\partial_{\kappa\lambda}U\Big) \\
O_5 &= \frac{1}{5!}\int dx\Big(U^5 + 3U^2\partial_\kappa U\partial_\kappa U + 2U\partial_\kappa U U\partial_\kappa U + U\partial_{\kappa\lambda}U\partial_{\kappa\lambda}U + \frac{5}{3}\partial_\kappa U\partial_\lambda U\partial_{\kappa\lambda}U \\
&\qquad + \frac{1}{14}\partial_{\kappa\lambda\mu}U\partial_{\kappa\lambda\mu}U\Big) \\
O_6 &= \frac{1}{6!}\int dx\Big(U^6 + 4U^3\partial_\kappa U\partial_\kappa U + 6U^2\partial_\kappa U U\partial_\kappa U + \frac{12}{7}U^2\partial_{\kappa\lambda}U\partial_{\kappa\lambda}U \\
&\qquad + \frac{9}{7}U\partial_{\kappa\lambda}U U\partial_{\kappa\lambda}U + \frac{26}{7}U\partial_{\kappa\lambda}U\partial_\kappa U\partial_\lambda U + \frac{26}{7}U\partial_\kappa U\partial_\lambda U\partial_{\kappa\lambda}U \\
&\qquad + \frac{17}{14}\partial_\kappa U\partial_\lambda U\partial_\kappa U\partial_\lambda U + \frac{18}{7}U\partial_\kappa U\partial_{\kappa\lambda}U\partial_\lambda U + \frac{9}{7}\partial_\kappa U\partial_\kappa U\partial_\lambda U\partial_\lambda U \\
&\qquad + \frac{3}{7}U\partial_{\kappa\lambda\mu}U\partial_{\kappa\lambda\mu}U + \partial_\mu U\partial_{\kappa\lambda}U\partial_{\kappa\lambda\mu}U + \partial_\mu U\partial_{\kappa\lambda\mu}U\partial_{\kappa\lambda}U \\
&\qquad + \frac{11}{21}\partial_{\kappa\lambda}U\partial_{\lambda\mu}U\partial_{\mu\kappa}U + \frac{1}{42}\partial_{\kappa\lambda\mu\nu}U\partial_{\kappa\lambda\mu\nu}U\Big)
\end{aligned} \tag{C.1}$$

where U is to replace by $U - a$ respectively $U_0 - a$. U and U_0 are given in eq. (3.13) and eq. (3.14).

References

[1] M. Dine, R.G. Leigh, P. Huet, A. Linde and D. Linde, Phys.Rev. **D46** (1992) 550

[2] G.W. Anderson and L.J. Hall, Phys.Rev. **D45** (1992) 2685

[3] D. Bödeker, W. Buchmüller, Z. Fodor and T. Helbig, DESY 93-147 (1993)

[4] A. Jakovác, K. Kajantie and A. Patkós, HU-TFH-94-01 (1994)

[5] B. Bunk, E.M. Ilgenfritz, J. Kripfganz, and A. Schiller, Phys.Rev.Lett. **B284** (1992) 371; Nucl.Phys. **B403** (1993) 453

[6] K. Kajantie, K. Rummukainen and M. Shaposhnikov, Nucl.Phys. **B407** (1993) 356

[7] J.S. Langer, Ann.Phys. **54** (1969) 258

[8] M.G. Schmidt and C. Schubert, Phys.Lett. **B318** (1993) 438

[9] D. Fliegner, M.G. Schmidt and C. Schubert, HD-THEP-93-44 (1993), Z.Phys., to be published

[10] M. Reuter and C. Wetterich, HD-THEP-93-40 (1993)

[11] U. Ellwanger, HD-THEP-94-2 (1994)

[12] N.P. Landsman, Nucl.Phys. **B322** (1989) 498

[13] J. Caro and L.L. Salcedo, Phys.Lett. **B309** (1993) 359

[14] E.J. Weinberg, Phys.Rev.**D47** (1993) 4614

[15] M.E. Shaposhnikov, Phys.Lett. **B316** (1993) 112

[16] M. Hellmund, J. Kripfganz and M.G. Schmidt, HD-THEP-93-23 (1993)

[17] I. Affleck, Phys.Rev.Lett **46** (1981) 388

[18] A.D. Linde, Nucl.Phys. **B216** (1983) 421

[19] K. Enqvist, J. Ignatius, K. Kajantie and K. Rummukainen, Phys.Rev. **D45** (1992) 3415

[20] B.H. Liu, L. McLerran and N. Turok, Phys.Rev. **D46** (1992) 2668

[21] A. Laser, diploma thesis, Heidelberg (1993)

[22] P.L. Csernai and J.I. Kapusta, Phys.Rev. **D46** (1992) 1379

[23] L. Carson, Phys.Rev. **D42** (1990) 2853

[24] L. Carson and L. McLerran, Phys.Rev. **D41** (1990) 647

[25] D.I. Diakonov, V.Y. Petrov and A.V. Yung, Phys.Lett.**B130** (1983) 385

[26] F. Schechter, diploma thesis, Heidelberg (1993)

[27] D. Fliegner, diploma thesis, Heidelberg (1994)

[28] W. Buchmüller, Z. Fodor, T. Helbig and D. Walliser, DESY 93-021 (1993)

[29] W.N. Cottingham, D. Kalafatis and R. Vinh Mau, IPNO/TH 93-03 (1993)

[30] J. Baacke and V.G. Kiselev, Phys.Rev. **D48** (1993) 5648

[31] M. Reuter and C. Wetterich, Nucl.Phys. **B408** (1993) 91

Tables

y	T	$\frac{\lambda_-}{(gv(T))^2}$	$\bar{S}$	$\ln\left(\frac{A}{T^4}\right)$	$\ln\left(\frac{R}{T^3}\right)$
0.1	72.58	-0.09 10^{-3}	2216.4	-154.	-2358.
0.2	72.56	-0.37 10^{-3}	558.1	-83.9	-632.6
0.3	72.53	-0.84 10^{-3}	244.3	-50.0	-286.4
0.4	72.49	-1.55 10^{-3}	131.5	-35.6	-160.5
0.5	72.44	-2.53 10^{-3}	77.3	-28.4	-100.2
0.6	72.38	-3.68 10^{-3}	46.4	-24.3	-66.2
0.7	72.30	-4.63 10^{-3}	26.8	-21.9	-45.2
0.8	72.21	-4.71 10^{-3}	13.6	-20.7	-31.8
0.9	72.11	-3.23 10^{-3}	4.8	-20.7	-24.5

Table 1: Numerical results for $\tilde{m}_H = \frac{1}{2}\tilde{m}_W$

y	T	$\frac{\lambda_-}{(gv(T))^2}$	$\bar{S}$	$\ln\left(\frac{A}{T^4}\right)$	$\ln\left(\frac{R}{T^3}\right)$
0.1	97.27	-0.14 10^{-3}	1086.9	-115.	-1191.
0.2	97.25	-0.58 10^{-3}	273.8	-82.0	-347.0
0.3	97.23	-1.33 10^{-3}	120.0	-50.6	-163.5
0.4	97.19	-2.45 10^{-3}	64.8	-36.7	-95.6
0.5	97.15	-4.00 10^{-3}	38.2	-29.5	-63.0
0.6	97.10	-5.86 10^{-3}	23.1	-25.4	-44.8
0.7	97.04	-7.44 10^{-3}	13.5	-23.0	-33.8
0.8	96.97	-7.65 10^{-3}	7.0	-21.8	-27.1
0.9	96.87	-5.21 10^{-3}	2.6	-22.0	-24.2

Table 2: Numerical results for $\tilde{m}_H = \frac{3}{4}\tilde{m}_W$

Figures

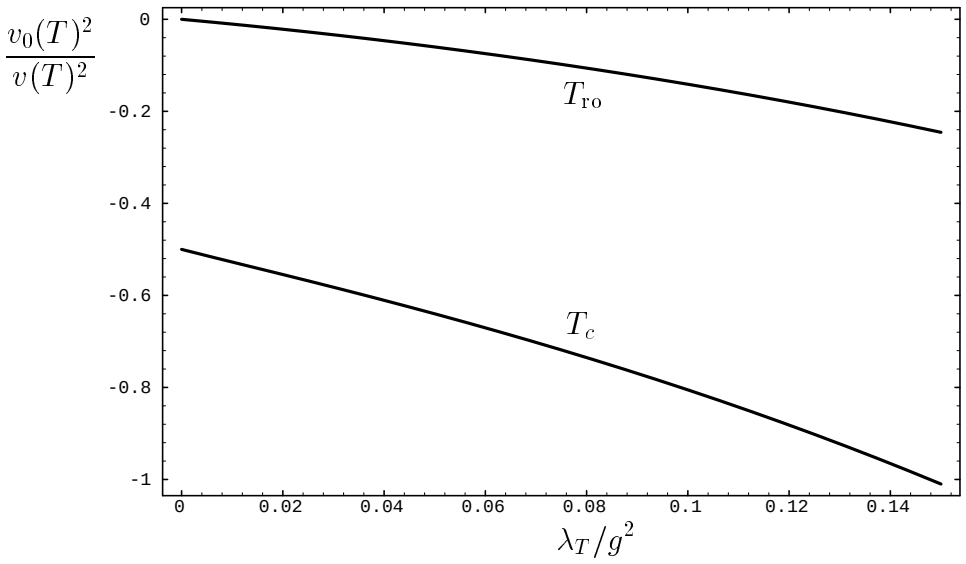

Figure 1: The parameter $\frac{v_0(T)^2}{v(T)^2}$ introduces the temperature dependence into the masses and the potential. It is plotted versus $\frac{\lambda_T}{g^2}$ at the critical and at the roll-over temperature. The plot range $0 \leq \frac{\lambda_T}{g^2} \leq 1.5$ covers the zero temperature Higgs mass range $0 \leq \tilde{m}_H \leq \tilde{m}_W$.

y	T	$\frac{\lambda_-}{(gv(T))^2}$	$\bar{S}$	$\ln\left(\frac{A}{T^4}\right)$	$\ln\left(\frac{R}{T^3}\right)$
0.1	123.85	-0.2 10^{-3}	593.7	-89.	-672.
0.2	123.84	-0.8 10^{-3}	149.5	-81.4	-222.7
0.3	123.82	-1.9 10^{-3}	65.5	-52.0	-111.1
0.4	123.79	-3.6 10^{-3}	35.4	-38.3	-68.5
0.5	123.76	-5.8 10^{-3}	21.0	-31.0	-47.9
0.6	123.72	-8.6 10^{-3}	12.8	-26.8	-36.5
0.7	123.67	-11.2 10^{-3}	7.6	-24.4	-29.8
0.8	123.60	-11.6 10^{-3}	4.0	-23.1	-26.0
0.9	123.52	-7.9 10^{-3}	1.5	-23.3	-25.0

Table 3: Numerical results for $\tilde{m}_H = \tilde{m}_W$

$\frac{\tilde{m}_H}{\tilde{m}_W}$	y_s	$\bar{S}$	$\ln\left(\frac{A}{T^4}\right)$	$\ln\left(\frac{A}{T^4}\right)/\bar{S}$
1/2	0.42	112.9	-33.4	0.295
3/4	0.33	101.2	-45.5	0.450
1	0.26	85.5	-61.6	0.720

Table 4: Relative onset-temperatures and corresponding values for different Higgs masses

	$\tilde{m}_H = \frac{1}{2}\tilde{m}_W$		$\tilde{m}_H = \frac{3}{4}\tilde{m}_W$		$\tilde{m}_H = \tilde{m}_W$	
$\frac{\sigma}{gv(T)^3}$	0.0219		0.0276		0.0338	
y	$\bar{S}$	$\bar{S}_{\rm TW}$	$\bar{S}$	$\bar{S}_{\rm TW}$	$\bar{S}$	$\bar{S}_{\rm TW}$
0.1	2216.4	2210.9	1086.9	1079.8	593.7	587.7
0.2	558.1	566.7	273.8	275.6	149.5	149.0
0.3	244.3	258.5	112.0	125.2	65.5	67.2
0.4	131.5	149.5	64.8	72.0	35.4	38.5
0.5	77.3	98.4	38.2	47.3	21.0	25.1
0.6	46.4	70.4	23.1	33.7	12.8	17.7
0.7	26.8	53.4	13.5	25.5	7.6	13.3
0.8	13.6	42.2	7.0	20.1	4.0	10.4
0.9	4.82	34.6	2.6	16.4	1.5	8.7

Table 5: The effective action of the critical bubbles in comparison with the thin-wall approximation values

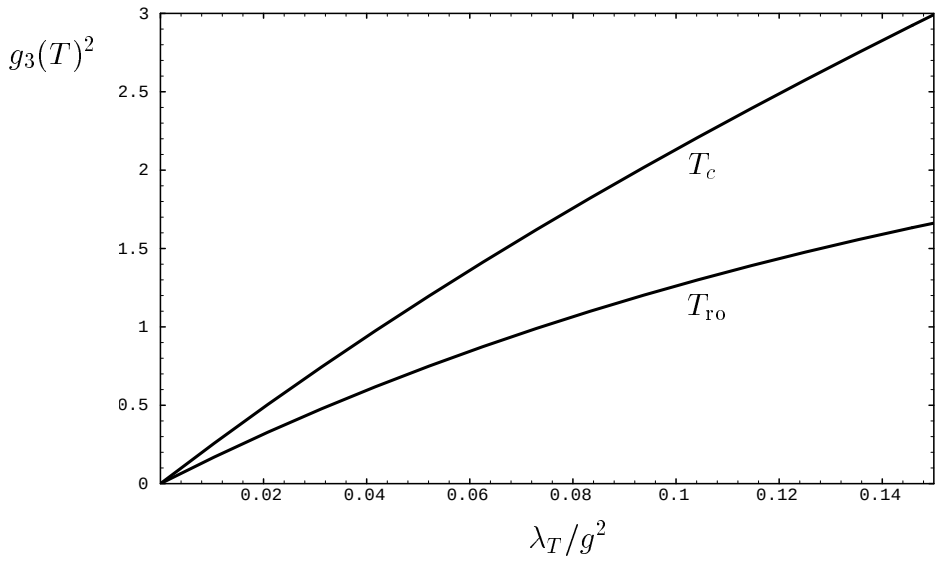

Figure 2: The effective 3-dimensional gauge coupling $g_3(T)^2$ versus $\frac{\lambda_T}{g^2}$ at the critical and at the roll-over temperature.

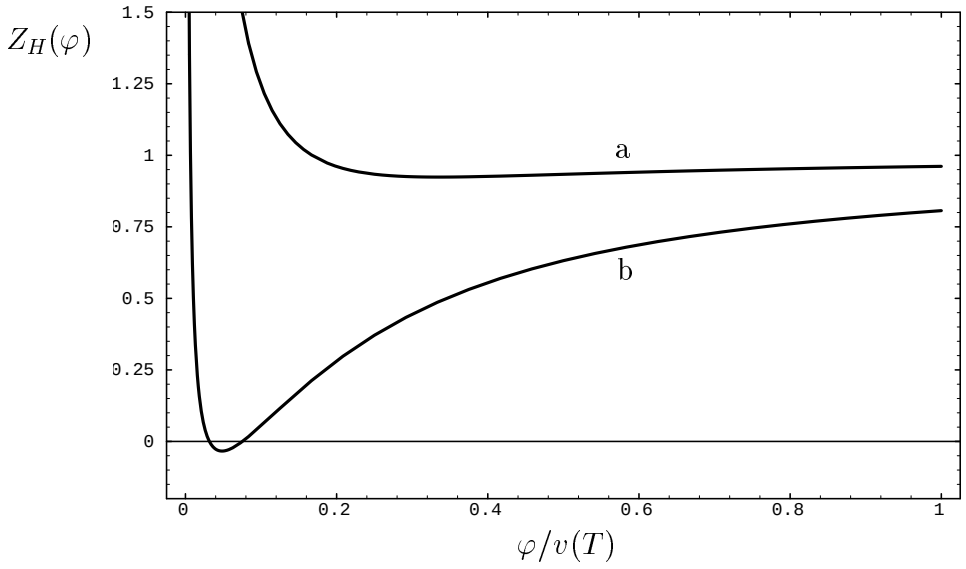

Figure 3: The Z-factor for the Higgs kinetic term Z_H versus φ in a) Landau and in b) 't Hooft-Feynman gauge. ($T = T_c$ and $\tilde{m}_H = \frac{1}{2}\tilde{m}_W$)

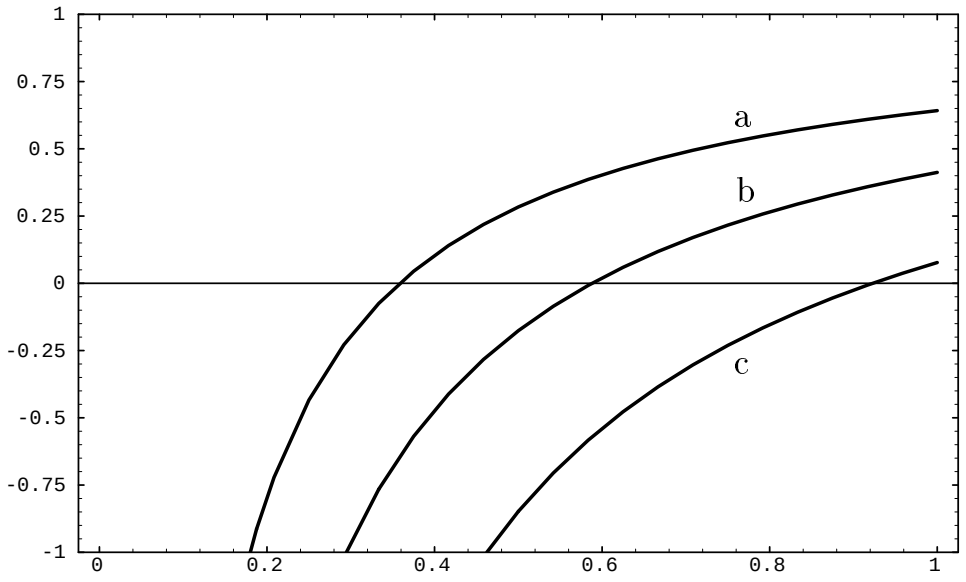

Figure 4: $Z_{\rm gauge}$ at the roll-over temperature for $\tilde{m}_H =$ a) $\frac{1}{2}\tilde{m}_W$, b) $\frac{3}{4}\tilde{m}_W$ and c) $\tilde{m}_W$.

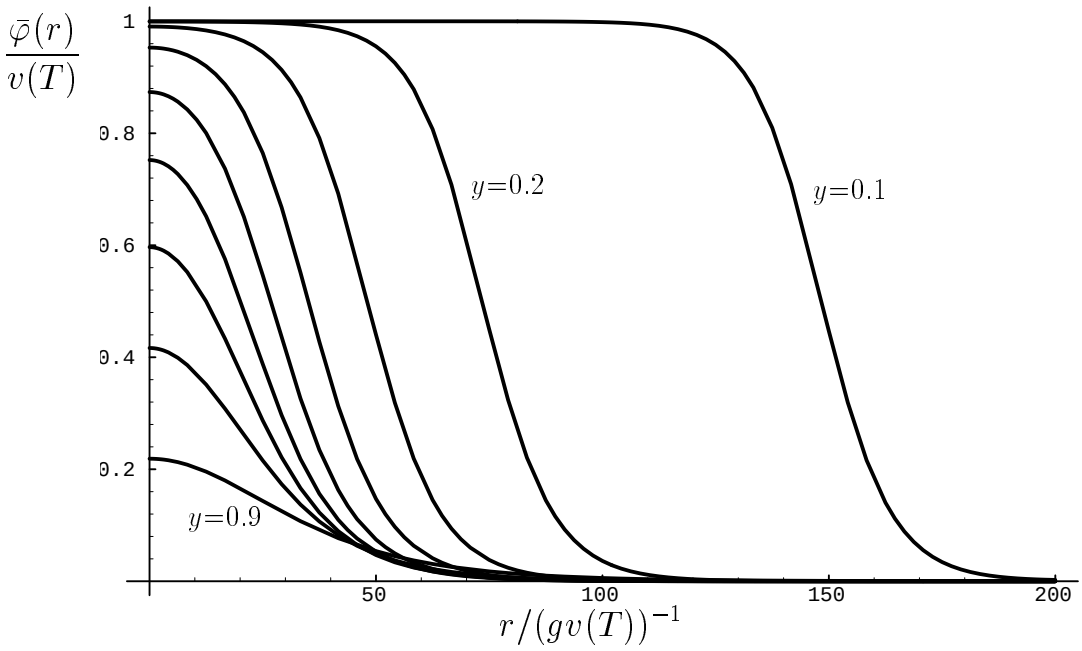

Figure 5: The critical bubbles are spherical symmetric. The profile functions are plotted for nine temperatures which are defined via the parameter y of eq. (3.9). ($\tilde{m}_H = \frac{1}{2}\tilde{m}_W$)

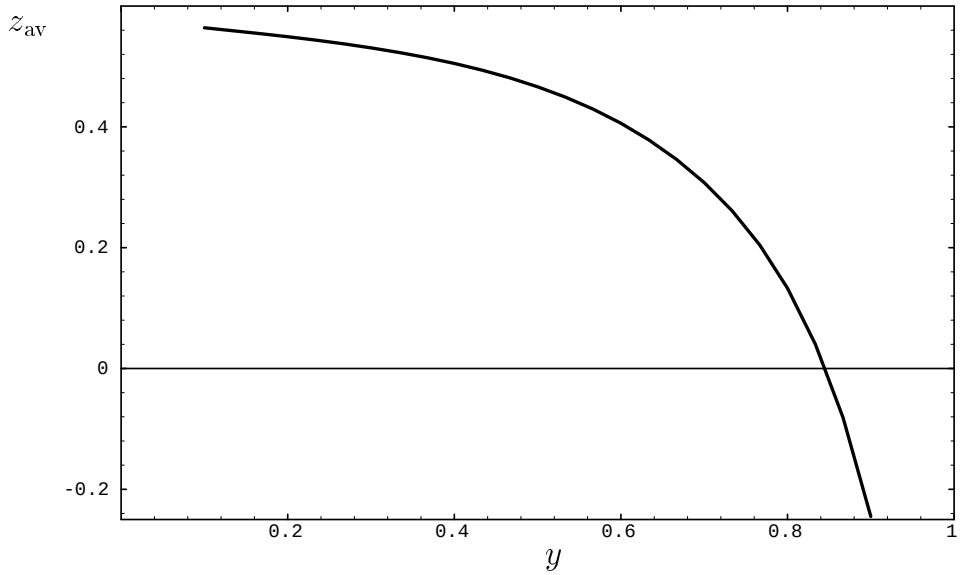

Figure 6: The average z defined in eq. (3.12) versus y. ($\tilde{m}_H = \frac{1}{2}\tilde{m}_W$)

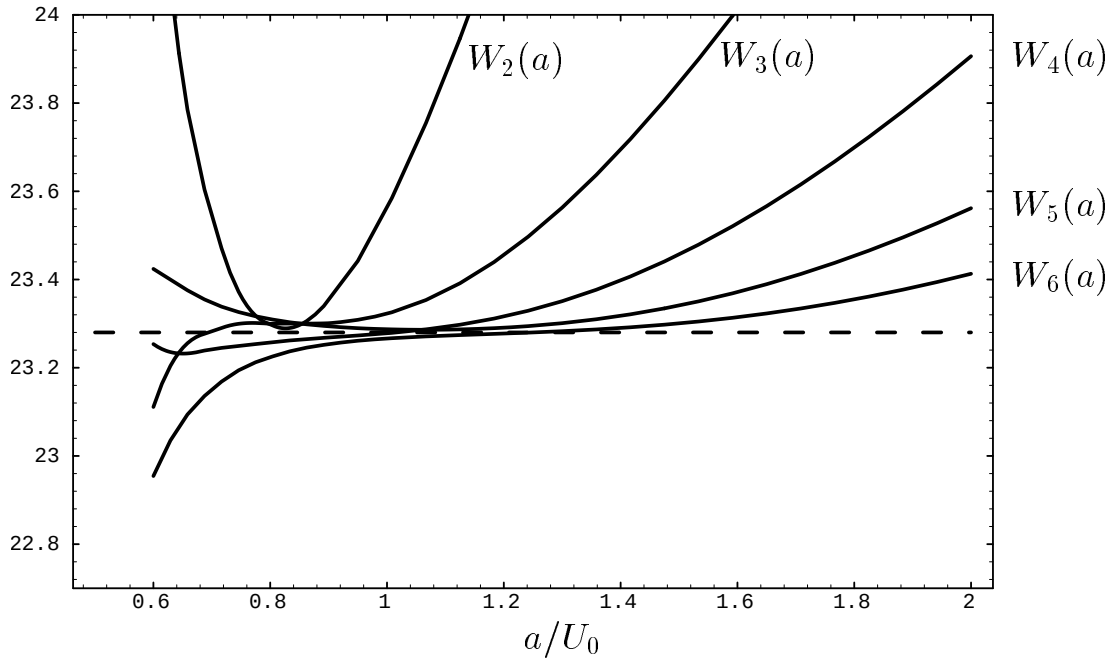

Figure 7: The functions $W_N(a)$ defined in equation (3.22) should converge towards a constant which is essentially the logarithm of the static prefactor. Here we give a typical plot of these functions. The dashed line is assumed to be the limit. ($\tilde{m}_H = \frac{1}{2}\tilde{m}_W$ and $y = 0.6$).

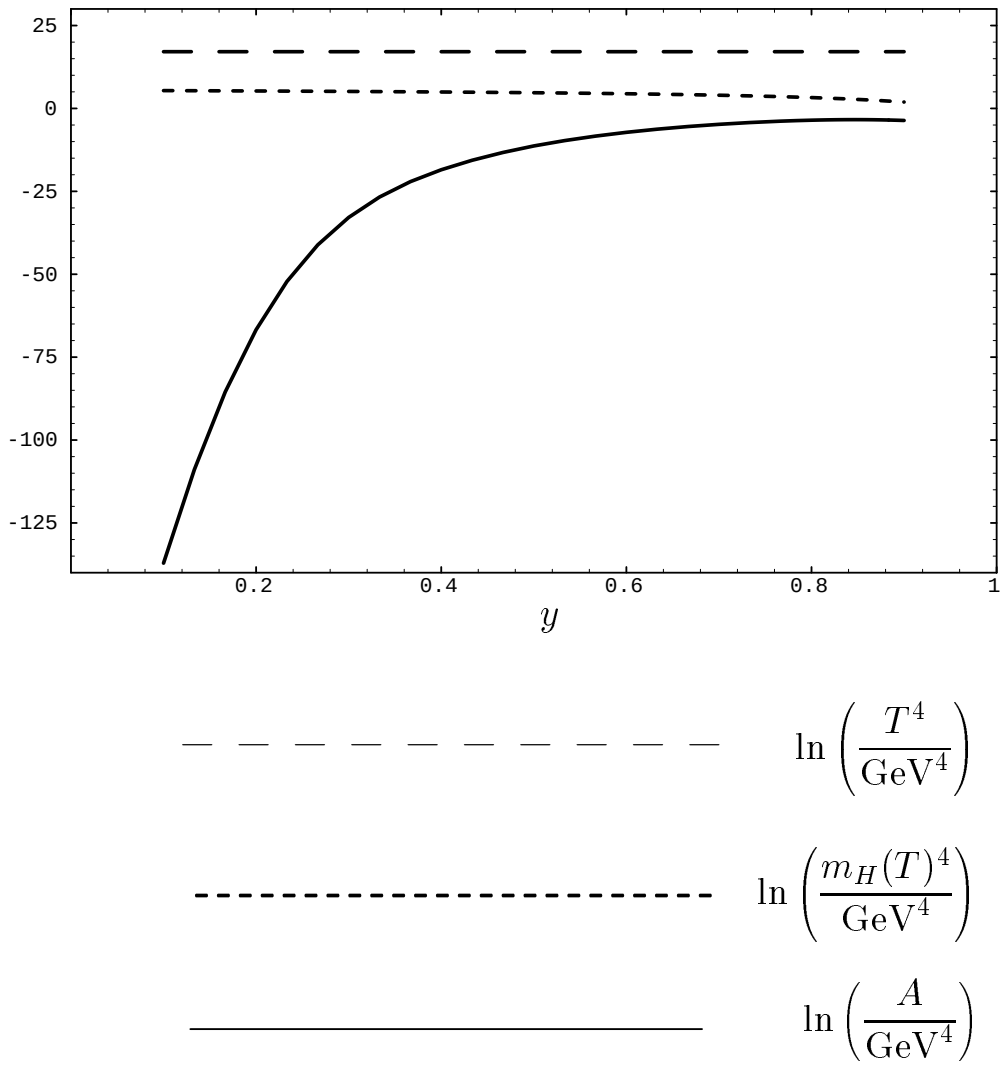

Figure 8: The static prefactor in comparison with dimensional estimates versus y. ($\tilde{m}_H = \frac{1}{2}\tilde{m}_W$).

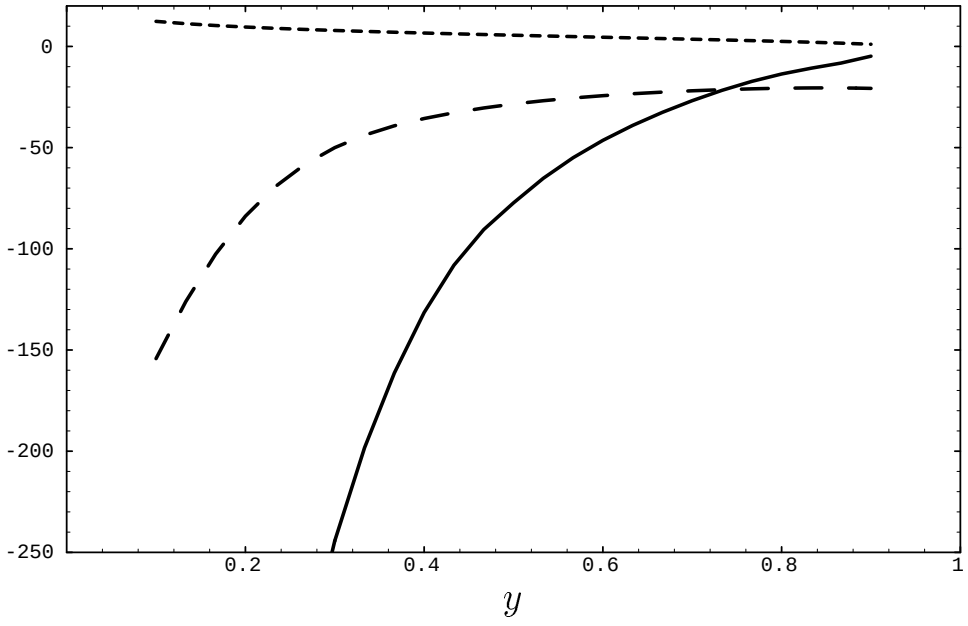

Figure 9: The summands of the logarithm of the nucleation rate (3.24). The main contributions are $-\bar{S}$ and $\ln\left(\frac{A}{T^4}\right)$. ($\tilde{m}_H = \frac{1}{2}\tilde{m}_W$)

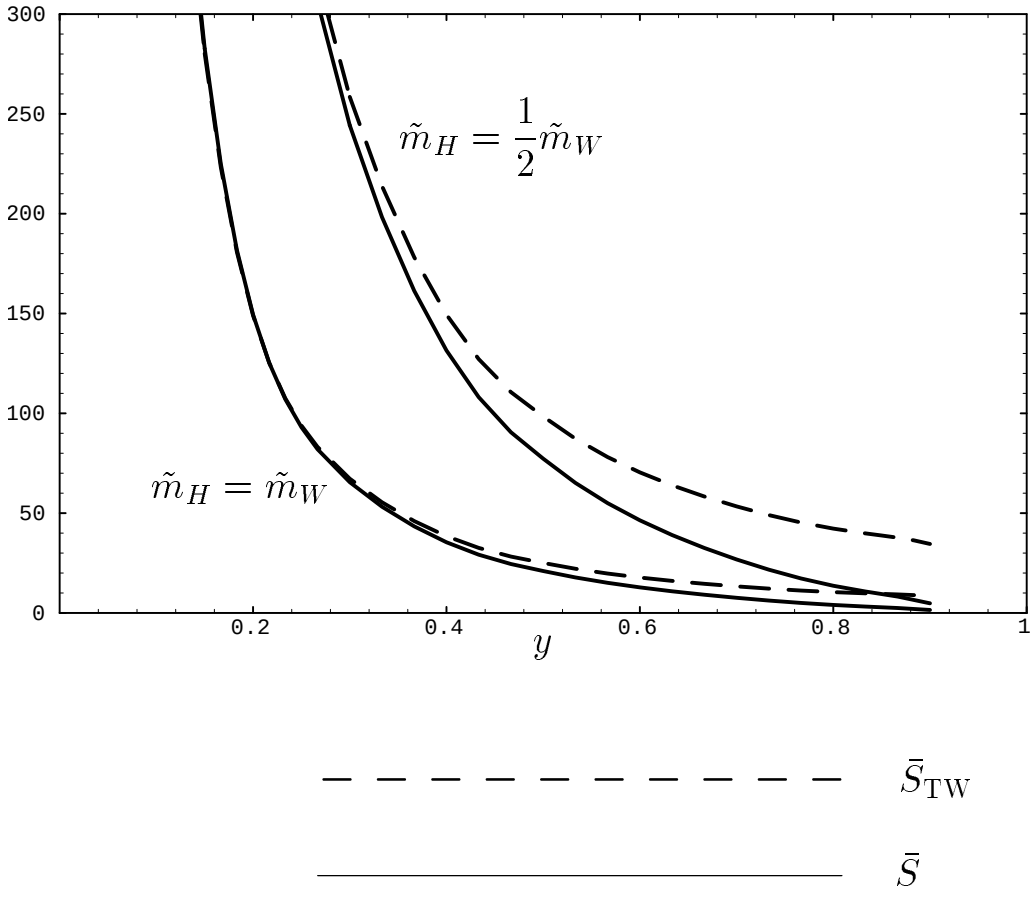

Figure 10: The effective action of the critical bubbles plotted in figure 5 in comparison with thin-wall estimates versus y.